STUK-A224 / DECEMBER 2007

A

Mobile Spectrometry for Source Finding and Prompt Reporting

S. Kuukankorpi, H. Toivonen, M. Moring, P. Smolander

Säteilyturvakeskus
Strålsäkerhetscentralen
Radiation and Nuclear Safety Authority

STUK

STUK-A224 / DECEMBER 2007

Mobile Spectrometry for Source Finding and Prompt Reporting

S. Kuukankorpi, H. Toivonen, M. Moring, P. Smolander

STUK • **SÄTEILYTURVAKESKUS**
STRÅLSÄKERHETSCENTRALEN
RADIATION AND NUCLEAR SAFETY AUTHORITY

Osoite/Address • Laippatie 4, 00880 Helsinki
Postiosoite / Postal address • PL / P.O.Box 14, FI-00881 Helsinki, FINLAND
Puh./Tel. +358 9 759 881 • Fax +358 9 759 88 500 • www.stuk.fi

The conclusions in the STUK report series are those of the of the authors and do not necessarily represent the official position of STUK.

ISBN 978-952-478-281-4 (print)
ISBN 978-952-478-282-1 (pdf)
ISSN 0781-1705

Edita Prima Oy, Helsinki 2007

Sold by:
STUK – Radiation and Nuclear Safety Authority
P.O.Box 14, FI-00881 Helsinki, Finland
Tel. +358-9-759 881
Fax +358-9-759 88500

KUUKANKORPI Satu, TOIVONEN Harri, MORING Mikael, SMOLANDER Petri. Mobile Spectrometry for Source Finding and Prompt Reporting. STUK-A224. Helsinki 2007, 42 pp + appendices 8 pp.

Key words: mobile gamma spectrometry, real-time automated analysis, peak significance, false positive rate, emergency preparedness, source finding, nuclear security

Abstract

The Finnish Radiation and Nuclear Safety Authority has developed a mobile laboratory for radiation safety and security applications. During source finding and monitoring missions, the laboratory utilises four *in-situ* gamma spectrometers working in 5 s acquisition intervals. The spectra are analysed immediately in the field and the results are automatically sent to a remote control centre for further processing. In operational spectrum analysis, a low false alarm rate is of paramount importance. A robust summation algorithm based on peak hypothesis testing was deployed. The algorithm is shown to work well with statistics fully under control when the baseline area under a tested peak is 20 counts or more.

KUUKANKORPI Satu, TOIVONEN Harri, MORING Mikael, SMOLANDER Petri. Mobiili spektrometrijärjestelmä lähteenetsintään ja tulosten välittömään raportointiin. STUK-A224. Helsinki 2007, 42 s + liitteet 8 s.

Avainsanat: mobiili gammaspektrometria, reaaliaikainen automaattianalyysi, piikkisignifikanssi, virhehavaintotaajuus, onnettomuuksiin varautuminen, lähteenetsintä, säteilyturva

Tiivistelmä

Säteilyturvakeskus (STUK) on kehittänyt mittausauton säteilyturvallisuussovelluksia ja säteilyturvatehtäviä varten. Auton laitteistoon kuuluvat neljä in-situ-gammaspektrometriä mittaavat kukin spektrejä viiden sekunnin aikavälein. Kaikki spektrit analysoidaan reaaliaikaisesti kentällä ja tulokset lähetetään automaattisesti STUKiin mahdollista jatkoprosessointia varten. Olennaisimpia vaatimuksia operatiivisiin säteilyvalvontatehtäviin soveltuvalle spektrianalyysille on, että se antaa mahdollisimman vähän vääriä hälytyksiä. Tätä tarkoitusta varten kehitettiin ja testattiin yksinkertainen mutta järeä piikkihypoteesitestiin perustuva summeerausalgoritmi. Tässä raportissa esitetyt testitulokset osoittavat, että algoritmi toimii luotettavasti ja ennustetun statistiikan mukaisesti, kun testattavan piikin taustassa[1)] on vähintään 20 pulssia.

[1)] Taustalla tarkoitetaan tässä englanninkielistä termiä baseline, jolle ei ole omaa suomenkielistä vastinetta.

Contents

Symbols

A	peak area
a	source activity, Bq
b	average baseline per channel
B	baseline area under the peak
B_1	number of counts in lower baseline calculation area
B_2	number of counts in upper baseline calculation area
c	ratio of measured to theoretical standard deviation of A
C	total counts in ROI
$D(A)$	standard deviation of peak area
$D^2(A)$	variance of peak area
$D(p)$	standard deviation of p, see below
f	gamma yield per disintegration
g	ratio of counts in peak calculation area to total counts in a Gaussian peak
$I(x)$	detected count rate at distance x, cps
k_α, k_β	Gaussian abscissa determined by the risk level α or β
$L_C(\alpha)$	Currie's decision limit
$L_D(\alpha)$	Currie's detection limit
MDA	minimum detectable activity, Bq
n	channels below each baseline calculation area
N	number of measured spectra
$P(S)$	Cumulative Gaussian probability distribution
P_0	Cumulative Gaussian probability at $S = 0$
p	ratio of counts in the upper baseline calculation area to counts in the lower baseline calculation area, B_2/B_1
S	peak significance
S_{offset}	average peak significance for a given ROI without a source ($E\{S_{offset}\} = 0$)
T	counting time, s
W	channels under the peak calculation area
x	vehicle to source distance
ε	absolute detection efficiency
μ	linear attenuation coefficient, 1/m

1 Introduction

The Finnish Radiation and Nuclear Safety Authority has developed a mobile laboratory called SONNI *(Sophisticated On-site Nuclear Identification)* for emergency preparedness and Nuclear Security [1]. SONNI is operated by a crew of four and is equipped with air sampling and sample measurement systems, including *in-situ* gamma spectrometry systems. SONNI has three different ways of communicating with headquarters: commercial GPRS and a TETRA-based Public Authority network called VIRVE and satellite. SONNI is capable of fallout mapping, source finding and, most importantly, communicating the results to the operations centre in real time.

Whilst in the field, SONNI produces a huge amount of data, especially when used for source finding. This data must be analysed in real time and possible findings must be communicated forward with minimum delay. Since continuous manual analysis of spectra arriving every few seconds is simply impossible, automation of the measurements, analyses and communication is required. The automated analysis must be fast and reliable, i.e. the frequency of false positives must be kept under control.

This document describes the summation analysis algorithm used for real-time gamma-spectrometry in SONNI and the logic in automated messaging. Test results and approximate detection distances are given for various gamma-emitting nuclides.

2 Detection system

The *in-situ* gamma spectrometry system of SONNI consists of three NaI(Tl) scintillation detectors and one electrically cooled HPGe. The NaI(Tl) detectors are wrapped in polyurethane to shield them against abrupt temperature changes; their temperature is constantly monitored with thermistors. Two of the NaI(Tl) detectors are 5 inches by 4 inch and are collimated to face left and right. The third, 2 inches by 2 inches NaI(Tl) detector is collimated with a 15° wide view straight ahead. The 58.5 mm by 66.5 mm size HPGe crystal is mounted on the ceiling with no collimation. This configuration of four detectors provides low detection limits, reliable identification and instant directional information.

The NaI(Tl) detectors are controlled with ORTEC digiBASE multichannel analysers mounted directly on the photomultiplier tube bases. The HPGe is controlled with DSPEC Pro from the same manufacturer. All data is collected with UniSAMPO [2] software and the spectra are saved in IMS 2.0 [3] format. *In-situ* measurements are carried out by continuously measuring spectra of equal acquisition time, typically five seconds, with all four detectors. These spectra are analysed, linked with location information and saved to the LINSSI [4] database in real time. The analysis results are automatically communicated to headquarters. In addition, the alarms are sent to the mobile (TETRA) phones of the key personnel in the operations centre. All data collecting, processing and storing is carried out with one Linux server (Liisa), whereas all automatic communication is left to another Linux server (Lille).

3 Summation algorithm for real-time spectrum analysis

There are a variety of programs capable of advanced spectrum analysis using the IMS 2.0 format spectra as input, including UniSAMPO itself. However, these are not used in SONNI. A separate script using a simple summation algorithm was developed for fast hypothesis testing of the presence of certain nuclides. This is justified for two reasons. First, real-time analysis with any advanced gamma spectrometric software puts too heavy a load on the computer server in fast *in-situ* measurements when each of the four detectors produces a gamma spectrum once every few seconds. Secondly, peak fitting is not a reliable method for peak area and significance calculations under the compromised statistics of a spectrum with short integration time. A simple summation over predefined regions of interest is a far more robust and faster method.

3.1 Analysis parameters

Prior to measurements, the analysis script is initialised with information on the summation parameters, nuclides for hypothesis testing, other energy intervals of interest and alarm limits. All this information is given in a specific initialisation file (Table I).

The minimum required signal that causes an alarm is defined separately for each signal type (roi or nuclide) with the *sInternal* parameter in the *Area* and *Nuclides* block. All alarms for a given signal type can be turned off by setting *sInternal* to -1, as is the case with K-40 in Table I. The parameter *sExternal* is used to define the signal level for outgoing automated messages on detection. For example, for Cs-137 in Table I, information on a signal with 0.8 < significance < 1 is not to be sent outside SONNI, but the SONNI crew should automatically be notified. The generation of automated messages is described in Chapter 5.

3.2 The algorithm

The hypothesis test is based on calculating the peak significance for each nuclide in the *Nuclides* block. The peak significance, *S,* is defined as the ratio of peak area *A* to Currie's decision limit [5] $L_C(\alpha)$,

$$S = \frac{A}{L_C(\alpha)} = \frac{A}{k_\alpha D(A)} \tag{1}$$

Table I. Initialisation file for the summation algorithm. The file is divided into three blocks. The *Area* block specifies alarm limits for pulse rates in the given energy intervals. The *Fit* block specifies the summation parameters for significance calculations (see Fig. 1), the area correction parameter, *g*, and the risk level for false positives in terms of the Gaussian abscissa, k_α. The *g* parameter is the ratio of counts covered with the summation parameters to total counts in a Gaussian peak. The *Nuclides* block lists all energy lines of interest for each nuclide to be tested together with energy uncertainties related to the peak location (temperature drifting). Alarm limits for nuclides are based on calculated significances and the *sInternal* and *sExternal* thresholds are used for signal classification in messaging. The last column, c, is used for correcting systematic errors in variance calculations (see Chapter 3.2).

Area					
areaId	*start (keV)*	*end (keV)*	*sInternal (cps)*	*sExternal (cps)*	
hiEnd	2750	3000	1.2	1.6	
Fit					
Peak Width (FWHM)	*Baseline Width (FWHM)*		*Baseline Distance (FWHM)*	*g*	k_α
1.2	0.6		1.2	0.842	4.753
Nuclides					
Nuclide	*Energy (keV)*	*Peak position uncertainty (keV)*	*sInternal*	*sExternal*	*c*
Am-241	59.54	3	0.8	1	1
Tc-99m	140.5	3	1	1.2	1
Ra-226	186.2	3	0.8	1	1
I-131	316.5	3	0.8	1	1
Ir-192	364.5	3	0.8	1	1
Cs-137	661.7	3	0.8	1	1
Co-60	1173.2	3	0.8	1	1
K-40	1460.8	6	-1	1	1

where $D(A)$ is the standard deviation of the peak area and k_α sets the risk level of detecting false positives in terms of the Gaussian abscissa. With $k_\alpha = 4.753$ the result $S > 1$ is a false positive once in a million measurements with no real activity present. The success of the hypothesis test relies on accurate non-biased peak area and variance estimation, i.e. there should be no systematic errors in the determination of either one of these.

The parameters of the summation algorithm are sketched in Fig. 1. All calculations are done in channels. The baseline is calculated from both sides of the area of interest according to *BaselineDistance* and *BaselineWidth* parameters. These two values are then added together and scaled with the number of channels under the peak (W) and under the baseline ($2n$) to get the baseline area B:

$$B = \frac{B_1 + B_2}{2n} W = bW \tag{2}$$

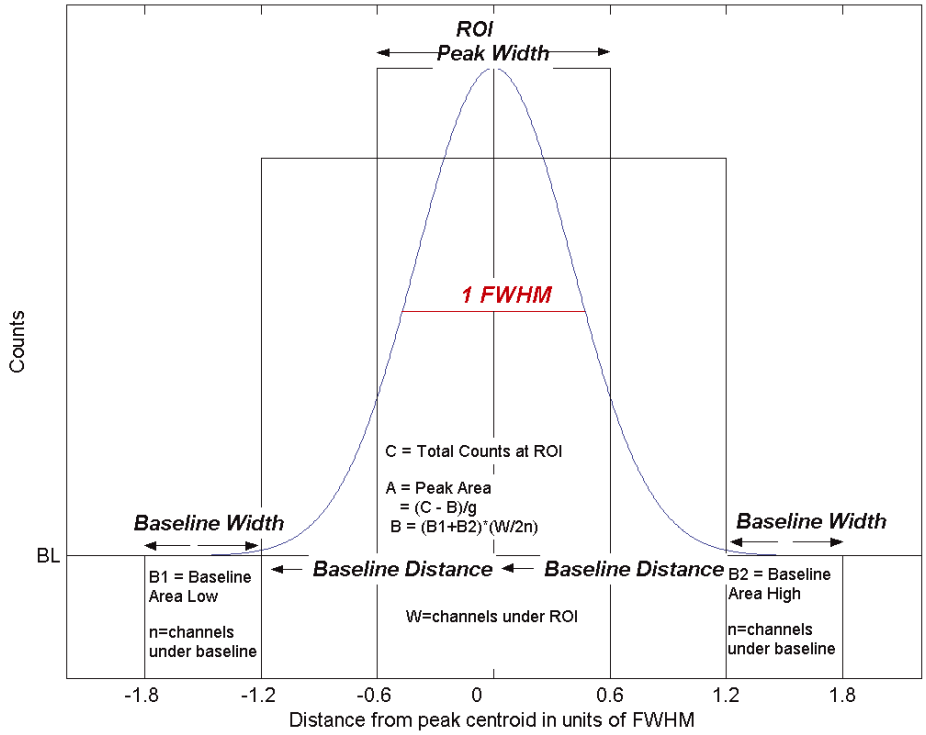

Fig. 1. Gaussian peak and summation parameters used for hypothesis testing. All parameters are given in units of FWHM. The peak area is calculated by subtracting the scaled baseline area from the total counts covered by the *PeakWidth*. If the *PeakWidth* does not span the whole Gaussian peak, the total counts in a peak is gained by scaling with the area correction parameter *g*. The parameters used for NaI(Tl) spectra are *PeakWidth* = 1.2, *BaselineWidth* = 0.6, *BaselineDistance* = 1.2 and g = 0.842. The parameters used to analyse HPGe spectra are *PeakWidth* = 2.5, *BaselineWidth* = 2.5 *BaselineDistance* = 2.5 and g = 1.

where B_1 and B_2 are defined as in Fig. 1 and b is the average baseline per channel. However, with NaI(Tl) detectors, the 1333 keV energy peak of Co-60 overlaps with the 1173 keV baseline calculation area B_2. Therefore, the baseline area of the 1173 keV Co-60 peak is only estimated from the counts in the B_1 area:

$$B = \frac{(1+p)B_1}{2n} W = bW \tag{3}$$

where $p = B_2/B_1$ depends on the shape of the background spectrum. Values of p are presented in Table II for the Helsinki area. The calculation of the standard deviation $D(p)$ from nearly 30,000 spectra shows that p is essentially a constant.

The peak area A is

$$A = \frac{C - B}{g} \tag{4}$$

where C is the total counts in ROI and g is the ratio of counts covered with *PeakWidth* to total counts in a Gaussian peak. The variance of the peak area $D^2(A)$ is estimated by

$$D^2(A) = \frac{1}{g^2}\left| A + B\left(1 + \frac{W}{2n}\right)\right| \tag{5}$$

except for Co-60 in the NaI(Tl) spectra, for which the variance is given by

$$D^2(A) = \frac{1}{g^2}\left| A + B\left(1 + \frac{(1+p)W}{2n}\right)\right| \tag{6}$$

Equations (5) and (6) provide a means to estimate the variance of the peak area; for small peaks, $A = 0$. Decision making on peak acceptance as a real finding depends on the accuracy of this estimation. Therefore, it is important to know the relationship between this theoretical variance and the real measured variance. The real measured variance is obtained from the peak area estimates provided by the hypothesis testing. The comparison was done with data measured in the Helsinki area at the beginning of August 2005. Table III presents the key results.

The first and foremost result is that the ratio (c) between the measured and the theoretical standard deviations is essentially close to 1. Hence the peak area variance is properly estimated using the simple theory presented in this paper.

Table II. Factor p (see Equation 3), its uncertainties and number of spectra used in calculating the baseline and its calculated standard deviation for Co-60 in the Helsinki area (see text).

Detector	Left NaI	Right NaI	Front NaI
p	0.6328	0.6489	0.5730
$D(p)$	0.0058	0.0076	0.0124
N	27 926	28 245	27 935

Since all measurement errors due to hardware failures and software malfunction were excluded from the data and the variance is calculated correctly enough, there should not be any false positives among the data for a risk level of 10^{-6} ($k_\alpha = 4.753$); i.e. the maximum detected significance, Max, should, on average, not exceed 1 more often than once in 1,000,000 measurements without a real source. Furthermore, the average detected significance, Avg, should be close to 0 when there is no real activity present. Still, there are a total of 9 false positives detected with the two big NaI(Tl) detectors with Tc-99m and Co-60, plus the average detected significance is around 0.2 for Tc-99m for all NaI(Tl) detectors. Since the variance is calculated correctly ($c \approx 1$) for these nuclides, these errors are explained with systematic errors in peak area calculation caused by poor energy resolution and spectrum shape, as described in Chapter 3.3.2. The presence of any real activity may also cause the average peak significance to deviate from zero. This is the case with Cs-137. The Chernobyl fallout is detected with HPGe ($Avg = 0.11$). The amount of Cs-137 in the field was small enough to be masked by a naturally occurring Bi-214 609.3 keV line in the large NaI(Tl) detectors due to the poor energy resolution.

Table III. Characteristics of calculated significances. The total number of analysed spectra was 26,990 for Left NaI(Tl), 27,170 for Right NaI(Tl), 24,252 for HPGe and 26,980 for Front NaI(Tl). All clear outliers were removed from the data. These included a total of 1,914 spectra with microphonics and 6 spectra with Tc-99m spikes. Two spectra with real Tc-99m signals with $S = 1.23$ and $S = 1.01$ were also excluded. The data is presented in blocks for each tested nuclide. *Ratio* is the fraction of cases with significance $S > 0$ compared to the total number of measurements. The *Max*, *Min* and *Avg* columns give the maximum, minimum and average significance with a standard deviation of *StdDev*. Type 1 lists all false positives. *AvgBase* and *AvgArea* give the average baseline and peak area. *StdDevReal* is the true measured standard deviation of the peak area, whereas *StdDevTheo* is the average of the theoretical, calculated standard deviation. *c* is the ratio of measured to theoretical standard deviation of the peak area and S_{offset} is the average significance *Avg* divided by *c*.

Am-241												
Detector	*Ratio*	*Max*	*Min*	*Avg*	*StdDev*	*Type 1*	*AvgBase*	*AvgArea*	*StdDevReal*	*StdDevTheo*	*c*	S_{offset}
Left	0.725	0.949	-0.552	0.123	0.192	0	127.420	11.345	17.963	19.396	0.926	0.133
Right	0.578	0.813	-0.622	0.049	0.193	0	105.569	3.822	16.308	17.523	0.931	0.052
HPGe	0.585	0.742	-0.595	0.047	0.191	0	15.579	1.134	4.859	5.068	0.959	0.049
Front	0.565	0.669	-0.505	0.065	0.177	0	6.376	1.307	4.021	4.546	0.885	0.074
Tc-99m												
Detector	*Ratio*	*Max*	*Min*	*Avg*	*StdDev*	*Type 1*	*AvgBase*	*AvgArea*	*StdDevReal*	*StdDevTheo*	*c*	S_{offset}
Left	0.847	1.090	-0.724	0.213	0.201	2	351.738	32.803	31.461	32.142	0.979	0.217
Right	0.894	1.047	-0.552	0.255	0.203	3	356.653	39.088	32.092	31.797	1.009	0.253
HPGe	0.603	0.842	-0.611	0.056	0.193	0	19.285	1.546	5.434	5.690	0.955	0.059
Front	0.860	0.927	-0.477	0.224	0.194	0	35.027	11.511	10.265	10.704	0.959	0.234
Ra-226												
Detector	*Ratio*	*Max*	*Min*	*Avg*	*StdDev*	*Type 1*	*AvgBase*	*AvgArea*	*StdDevReal*	*StdDevTheo*	*c*	S_{offset}
Left	0.435	0.782	-0.729	-0.027	0.200	0	353.220	-4.377	30.611	31.648	0.967	-0.028
Right	0.469	0.834	-0.778	-0.009	0.199	0	329.546	-1.547	29.370	30.568	0.961	-0.009
HPGe	0.626	0.798	-0.588	0.076	0.190	0	12.516	1.748	4.387	4.602	0.953	0.080
Front	0.706	0.818	-0.614	0.111	0.195	0	43.900	5.897	10.657	11.162	0.955	0.116

Ir-192												
Detector	*Ratio*	*Max*	*Min*	*Avg*	*StdDev*	*Type 1*	*AvgBase*	*AvgArea*	*StdDevReal*	*StdDevTheo*	*c*	S_{offset}
Left	0.430	0.775	-0.821	-0.031	0.200	0	191.555	-3.677	22.260	22.984	0.969	-0.032
Right	0.380	0.683	-0.902	-0.059	0.198	0	181.276	-6.656	21.512	22.290	0.965	-0.062
HPGe	0.548	0.687	-0.515	0.046	0.182	0	4.040	0.631	2.507	2.677	0.937	0.049
Front	0.506	0.723	-0.781	0.007	0.193	0	24.219	0.109	7.931	8.345	0.950	0.008
I-131												
Detector	*Ratio*	*Max*	*Min*	*Avg*	*StdDev*	*Type 1*	*AvgBase*	*AvgArea*	*StdDevReal*	*StdDevTheo*	*c*	S_{offset}
Left	0.503	0.740	-0.695	0.004	0.200	0	165.396	0.170	20.703	21.465	0.965	0.004
Right	0.519	0.877	-0.719	0.014	0.200	0	154.728	1.230	20.076	20.757	0.967	0.015
HPGe	0.537	0.714	-0.481	0.043	0.180	0	3.170	0.540	2.232	2.392	0.933	0.046
Front	0.525	0.743	-0.595	0.018	0.192	0	19.803	0.480	7.187	7.597	0.946	0.019
Cs-137												
Detector	*Ratio*	*Max*	*Min*	*Avg*	*StdDev*	*Type 1*	*AvgBase*	*AvgArea*	*StdDevReal*	*StdDevTheo*	*c*	S_{offset}
Left	0.197	0.662	-0.973	-0.176	0.205	0	89.823	-13.944	16.359	15.729	1.040	-0.169
Right	0.260	0.789	-0.980	-0.131	0.206	0	76.797	-9.627	15.000	14.407	1.041	-0.125
HPGe	0.670	0.691	-0.384	0.117	0.178	0	1.068	1.085	1.691	1.637	1.033	0.113
Front	0.526	0.662	-0.523	0.025	0.188	0	7.580	0.416	4.504	4.766	0.945	0.027
Co-60												
Detector	*Ratio*	*Max*	*Min*	*Avg*	*StdDev*	*Type 1*	*AvgBase*	*AvgArea*	*StdDevReal*	*StdDevTheo*	*c*	S_{offset}
Left	0.743	1.064	-0.635	0.140	0.206	2	36.797	7.778	12.000	12.163	0.987	0.142
Right	0.753	1.069	-0.604	0.146	0.208	2	32.646	7.680	11.458	11.519	0.995	0.147
HPGe	0.488	0.553	-0.336	0.019	0.156	0	0.638	0.162	1.041	1.078	0.965	0.019
Front	0.683	0.696	-0.419	0.118	0.195	0	2.573	1.610	3.320	3.414	0.972	0.121

A neat way to exclude the bias in the peak area is to define a new parameter, S_{offset}:

$$S_{offset} = \frac{Avg}{c} \tag{7}$$

where $c \approx 1$ for all cases other than Am-241 and the front NaI(Tl) detector. The S_{offset} describes the deviation of the significance from zero due to a biased peak area. Furthermore, it can be used to adjust the decision limit when locating sources in fallout areas. The Equation (1) takes the form:

$$S = \frac{A}{k_\alpha cD(A)} - S_{offset} \tag{8}$$

The theoretical cumulative probability of false positives as a function of the peak significance threshold with risk level α can be calculated for a Gaussian distribution with a mean value of 0.5 using the error function *erf**:

$$P(S > S_{treshold}) = \frac{1 - erf(S_{treshold})}{2} = \frac{1}{2} - \frac{1}{\sqrt{\pi}} \int_0^{S_{treshold}} e^{-t^2} dt \tag{9}$$

where

$$t = \frac{k_\alpha S}{\sqrt{2}} \tag{10}$$

The measured complementary cumulative probability distribution is calculated from the real data as:

$$P(S > S_{treshold}) = \frac{N(S > S_{treshold})}{N} \tag{11}$$

where N is the total number of measurements and $N(S > S_{treshold})$ is the number of cases where the measured significance is greater than the assumed significance threshold. The theoretical cumulative probability distribution is plotted together with the measured cumulative probability distribution for all tested nuclides in Figures 2–8. As can be seen, the curves for the left and right NaI(Tl) detectors follow the theoretical curve quite nicely, whereas the HPGe and front NaI(Tl) detector curves notably deviate as the energy of the tested gamma line increases. This behaviour is discussed in Chapter 3.3.3.

*Matlab©

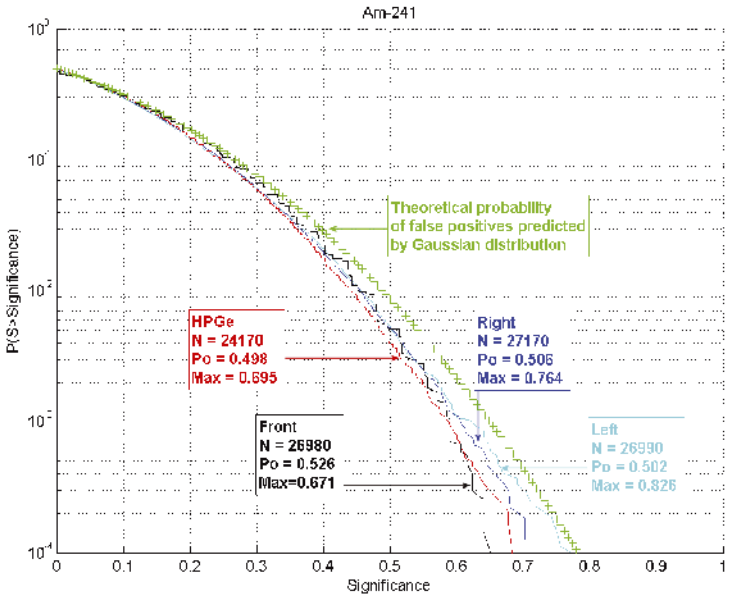

Fig. 2. Cumulative probability of false positives as a function of peak significance threshold for Am-241 with S_{offset} taken into account and correction c = 0.9 for front NaI(Tl). N is the total number of analysed spectra, P_0 is the cumulative probability of false positives at threshold S = 0 and Max is the maximum detected significance.

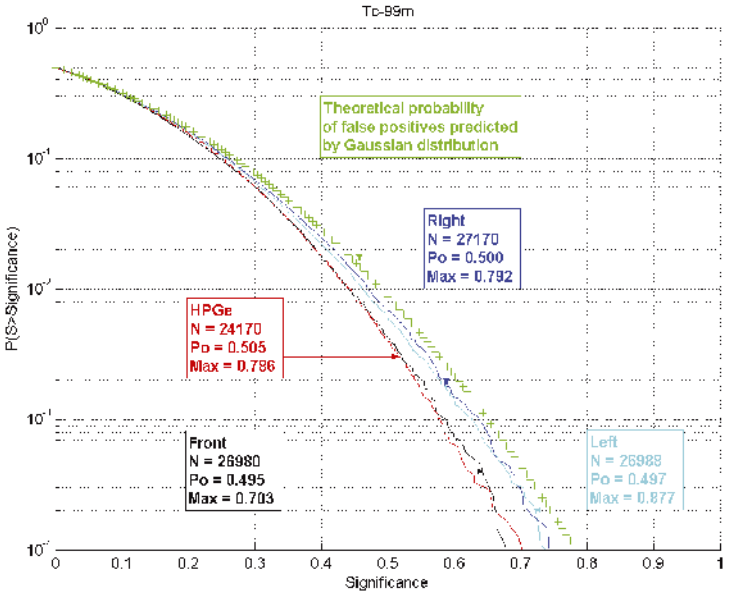

Fig. 3. Cumulative probability of false positives forTc-99m with S_{offset} taken into account. For symbols, see Fig. 2.

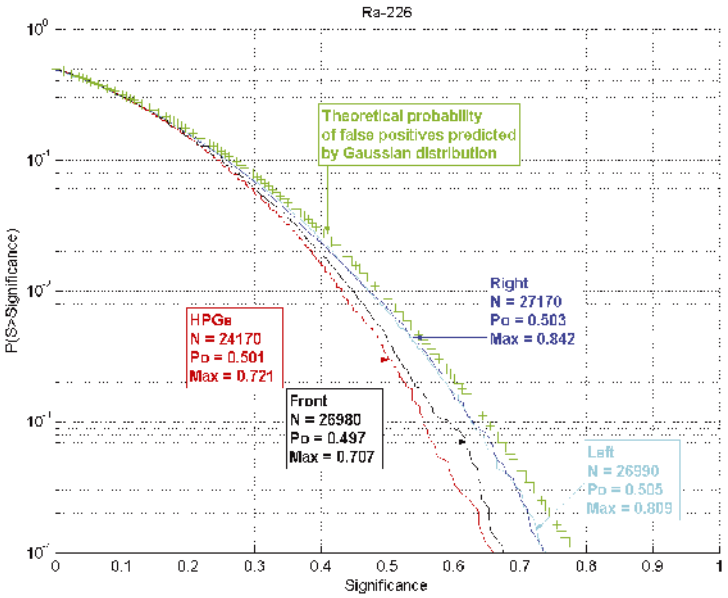

Fig. 4. Cumulative probability of false positives for Ra-226 with S_{offset} taken into account. For symbols, see Fig. 2.

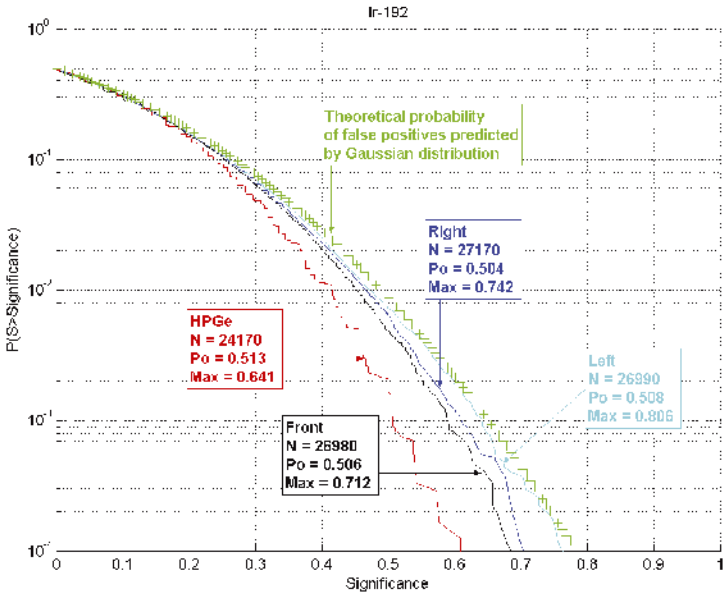

Fig. 5. Cumulative probability of false positives for Ir-192 with S_{offset} taken into account. For symbols, see Fig. 2.

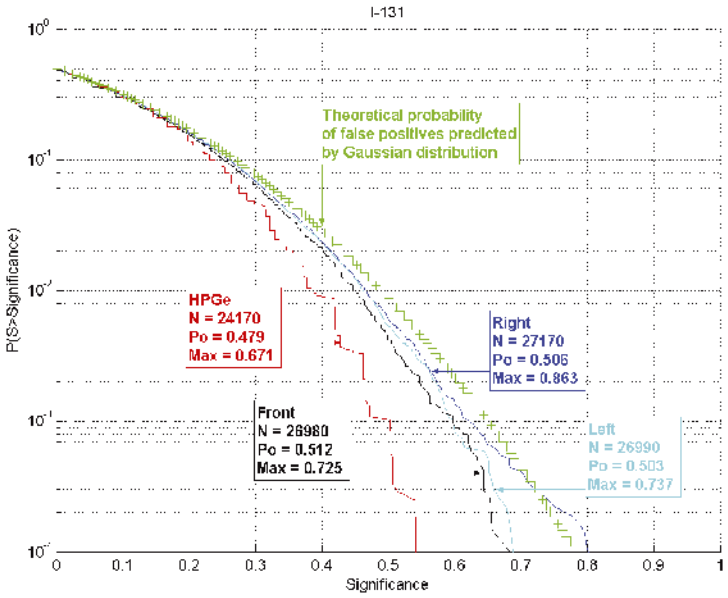

Fig. 6. Cumulative probability of false positives for I-131 with S_{offset} taken into account. For symbols, see Fig. 2.

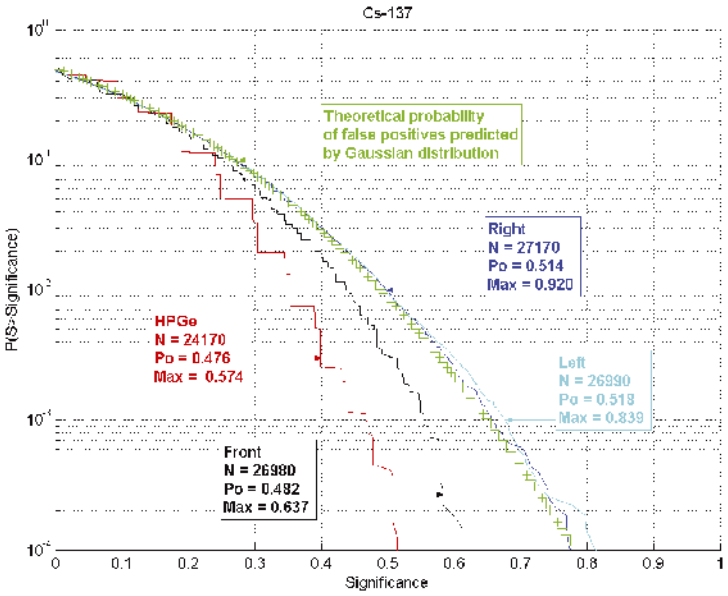

Fig. 7. Cumulative probability of false positives for Cs-137 with S_{offset} taken into account. For symbols, see Fig. 2

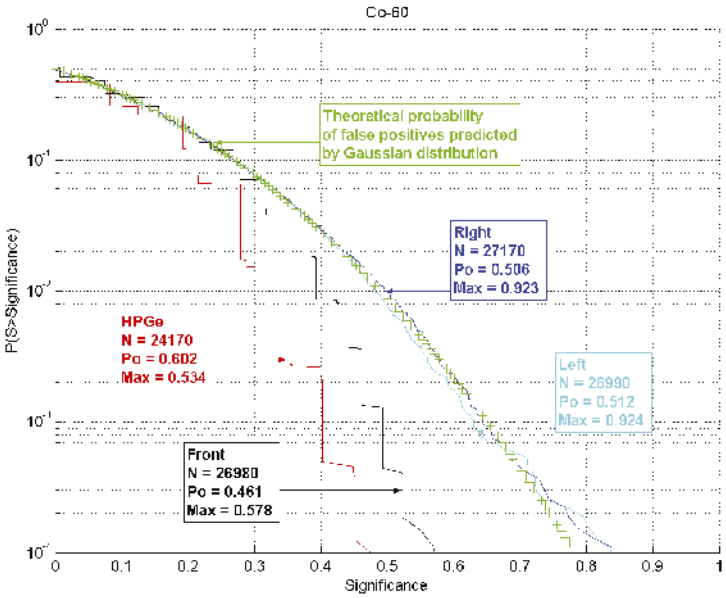

Fig. 8. Cumulative probability of false positives for Co-60 with S_{offset} taken into account. For symbols, see Fig. 2.

3.3 Sources of error

There are three main reasons for erroneous analysis results: hardware and software failures during measurements and systematic errors in peak area calculation. In addition, false negatives occur when count rates fall very low.

3.3.1 Errors in measurements

The quality of the measurements is only as good as the quality of the data acquisition electronics and software. Any disturbance in either of these may have an influence on the analysis results.

The main reason for false positives with the *in-situ* HPGe detector is its sensitivity to vibrations. In short, bumps in the road cause variable microphonic disturbances in the spectra. Figure 9 shows this effect at its worst, extending up to 1660 keV. The effect can be reduced with appropriate fastenings between the detector and the ceiling, but when it does occur it is possible that one of the spikes coincides with the peak or baseline area of a tested nuclide and gives a false positive or a false negative finding.

The NaI(Tl)-part of the system has its own problem: around once in 10,000 spectra one of the 1024 channels gets a huge number of counts (Fig. 10).

The following spectrum has negative counts in the same channel, cancelling the previous spike (Fig. 11). In fact, if the two spectra are added together, no irregularities can be seen. The impact on false positives or negatives in a single measurement is nevertheless irritating, as is the case with HPGe and microphonics. This failure is caused by a disturbance in the data collection. Each spectrum slice is saved as the difference between the total measured counts since the beginning of a mission and the total measured spectrum 5 seconds earlier. The spike occurs when the software fails in the subtraction for one channel due to a communication break with the hardware and assigns all the counts recorded so far to that very channel. The negative counts follow in the next spectrum as the spike is subtracted from the next, normal spectrum. The error is under repair.

Under heavy load the Linux server may slow down so badly that the data acquisition and database input form a bottleneck. If either one cannot be done in the 5-second time frame, the continuously acquired pulses are distributed unevenly between the 5-second spectra and form stripes in waterfall plots, as can be seen in Figure 12. A virtual 10-second spectrum gets divided in two so that the first spectrum gets 60–90% of the total pulses and the second the rest of them. Still, both of the spectra get recorded with 5-second integration time. In the worst case, the division of pulses starts in the middle of the spectrum. Figures 10 and 11 are an example of this uneven pulse distribution starting from the spiked channel. These stripes can cause both false total count rates and false nuclide identification alarms.

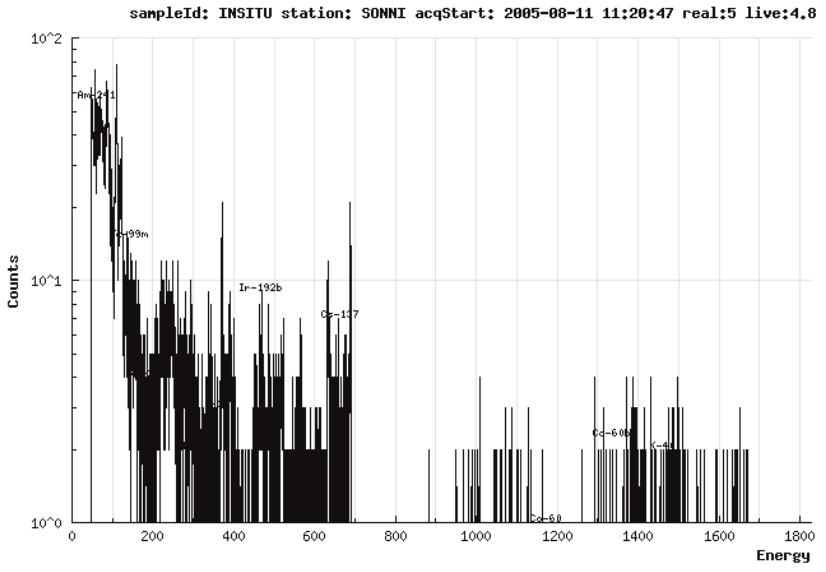

Fig. 9. Worst-case microphonics in HPGe.

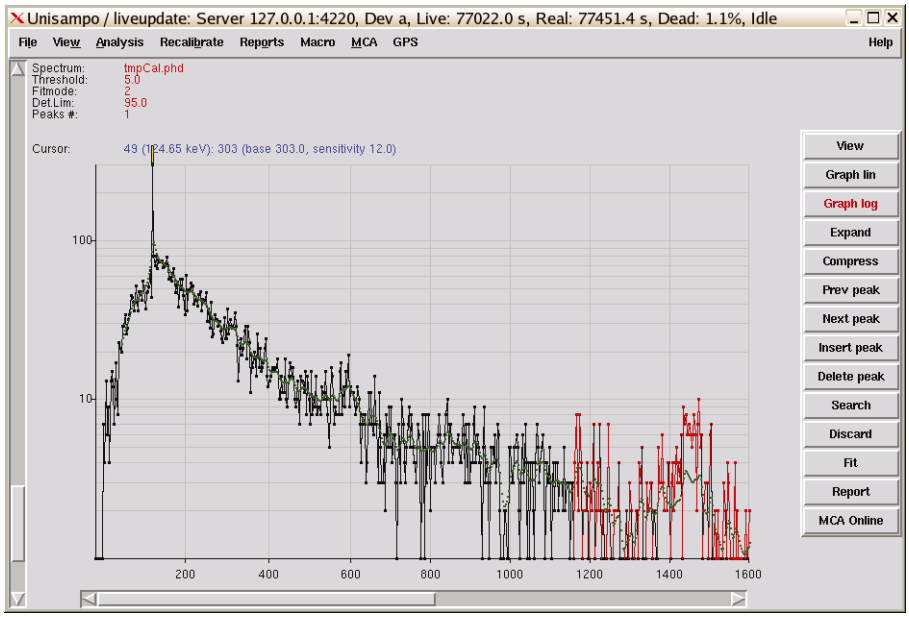

Fig. 10. Spike in Tc-99m peak calculation area detected with NaI(Tl). All channels after the spike have received some pulses from the following spectrum (see Fig. 11 as well).

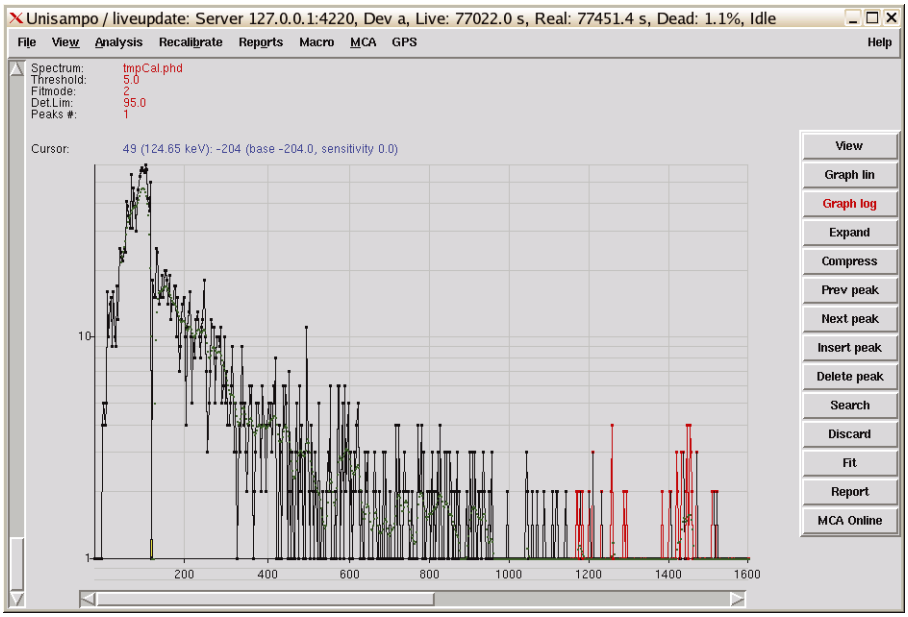

Fig. 11. Negative spike and lacking pulses after channel no 49 in the following spectra.

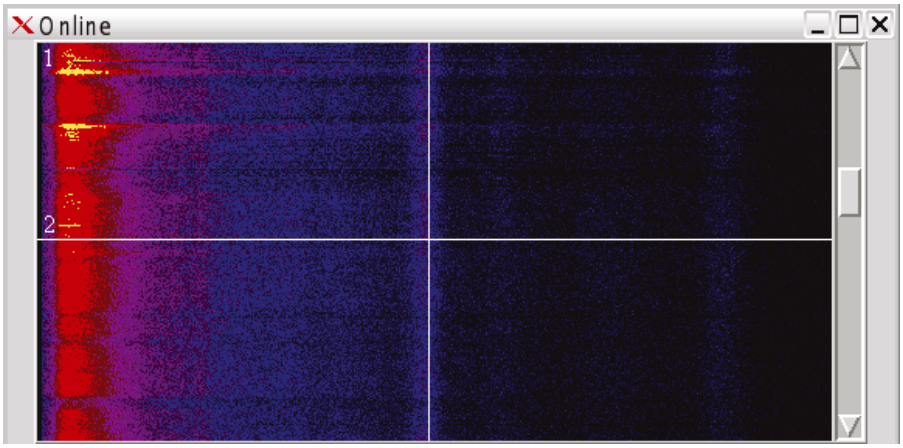

Fig. 12. Stripes as seen in a waterfall plot. Each horizontal pixel line represents one spectrum. 1) Location of spectra in Fig. 10 and 11. 2) A real signal from a Tc-99m source.

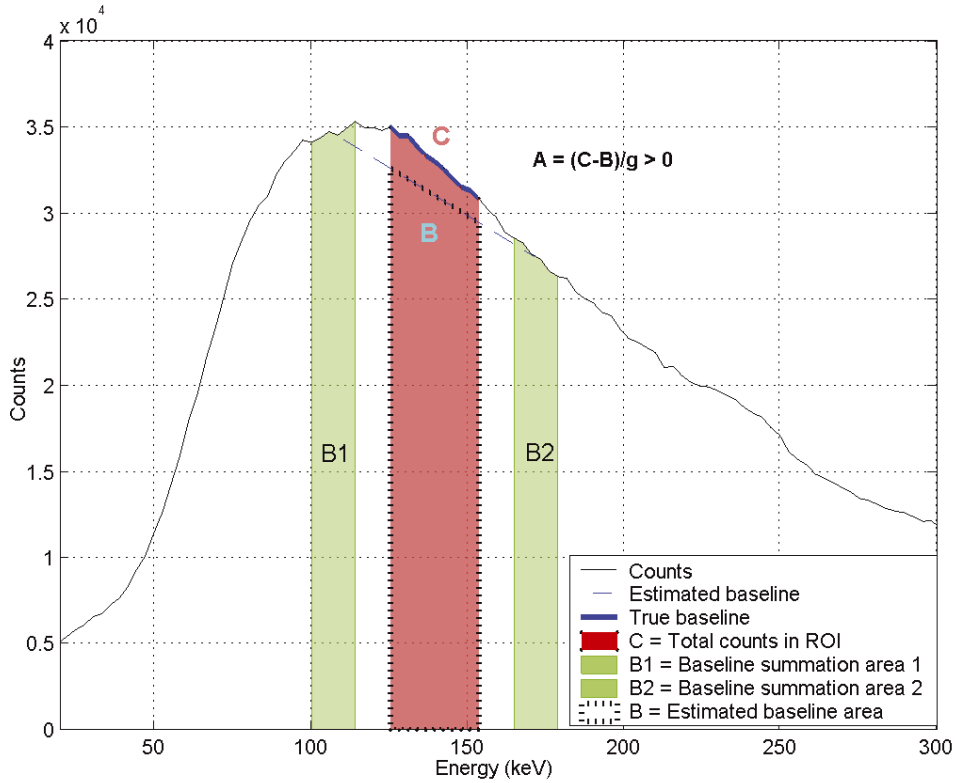

Fig. 13. Erroneous baseline estimation for Tc-99m in a background spectrum.

3.3.2 Errors in analysis

Limited energy resolution and temperature changes cause errors in peak area estimation, especially with NaI(Tl) detectors. Apart from Tc-99m, the deviations from zero of the average peak area in Table III are caused by naturally occurring isotopes with energy lines overlapping the peak and baseline calculation areas. For example, the Pb-214 351.9 keV line intrudes on the I-131 peak and Ir-192 baseline calculation areas, leaving the average significance for I-131 364.5 keV line positive and the Ir-192 316.5 keV line negative. Although these deviations can be handled in a known background by substituting the average significance in Equation (8), this may still cause a few false positives or negatives if the background or detector temperature changes drastically.

The case with Tc-99m is slightly different: the algorithm assumes a linear baseline, which does not hold for the summation area of the 140.5 keV line in the NaI(Tl) spectra. This is due to the slope around 120 keV. The peak and baseline calculation areas for Tc-99m are highlighted in a normal 80-minute background spectrum in Fig. 13. Since the baseline estimate falls below the real baseline, the calculated peak area is positive even if there is no peak. The overestimation of the peak area leads to more false positives than decision limit $S > 1$ with a $k_\alpha = 4.753$ risk would indicate. However, this is taken care of by adding S_{offset} to alarm limits.

3.3.3 Low background

The equations presented in Chapter 3.2. only work as predicted under Gaussian statistics, id est, with an average baseline area of at least around 20 counts. As can be clearly seen from Figures 2–8, the false positives cumulative probability curves for the HPGe and the smaller (front) NaI(Tl) detector fall far below the theoretical curve. Table III shows that for HPGe, only Tc-99m has a sufficient average baseline. The smaller NaI(Tl) has a large enough average baseline for Tc-99m, Ra-226, Ir-192 and I-131.

As the cumulative probability curves show, applying Equations (1)–(8) for too low count rates does not give any extra false positives. Instead, the approach leads to false negatives. From Equations (5) and (1) for $S \geq 1$ we get

$$A \geq \frac{k_\alpha^2 + \sqrt{k_\alpha^4 + 4 * \left(1 + \frac{W}{2n}\right) B k_\alpha^2 g^2}}{2g^2} \tag{12}$$

Equation (12) is far too conservative leading to false negatives as shown by the following simple calculus. Let us estimate A using HPGe detector under low background conditions, i.e., $B = 1$ which is typical of some regions for Cs-137. Then, because $k_\alpha = 4.753$, $W/2n = 0.5$ and $g = 1$, $A \geq 24$ counts. This is a huge signal. The overestimation implemented in Equation (12) is based on the conservative form of Equations (5) and (6); theoretically, the variance calculus should not contain the peak area A itself; for small signals this is expected to be near zero. Setting $A = 0$ in Equation (5) we get

$$A \geq \frac{k_\alpha \sqrt{B(1+\frac{W}{2n})}}{g} \tag{13}$$

Now we have a more realistic detection limit: $A \geq 6$ counts for the example above.

The low background statistics are a difficult domain of detection limit calculus. On the one hand, we do not want to have false alarms, on the other hand, we need good detection capability also at low count rates. Adoption of Poissonian statistics provides some advantages but also rules need to be developed on choosing the methods for certain conditions.

4 Detection Limits

4.1 Am-241, Tc-99m, Cs-137 and Co-60

Net peak count rates per GBq for each *in-situ* detector were measured at Vesivehmaa airfield in May 2005 using four different nuclides and distances. The results are presented in Table IV.

Table IV. Net count rate per GBq as a function of distance between source and origo. Note that the SONNI was placed so that HPGe was fixed at the origo and the distance is defined as distance from origo. Therefore, the distance between left and right NaI(Tl) detectors and the source is always 70 cm shorter than the tabulated values. Similarly, the distance between the front NaI(Tl) and the source is 2.5m shorter. The uncertainty estimates are dominated by the uncertainty of the source activities.

Am-241 cps/GBq for 59.54 keV line				
Distance (m)	*Left NaI(Tl)*	*Right NaI(Tl)*	*Front NaI(Tl)*	*HPGe*
20	85.5 ± 5%	88.0 ± 5%	20.5 ± 5%	20.1 ± 5%
40	15.1 ± 5%	14.9 ± 5%	4.43 ± 5%	3.76 ± 5%
80	1.73 ± 5%	1.80 ± 5%	0.534 ± 5%	0.353 ± 6%
120	0.310 ± 6%	0.348 ± 5%	0.0913 ± 6%	0.0520 ± 13%
Tc-99m cps/GBq for 140.5 keV line				
Distance (m)	*Left NaI(Tl)*	*Right NaI(Tl)*	*Front NaI(Tl)*	*HPGe*
20	1000 ± 5%	1110 ± 5%	115 ± 5%	187 ± 5%
40	182 ± 5%	199 ± 5%	30.7 ± 5%	37.4 ± 5%
80	21.0 ± 6%	22.0 ± 6%	4.18 ± 7%	3.79 ± 6%
120	6.16 ± 9%	no data	no data	0.833 ± 11%
Cs-137 cps/GBq for 661.7 keV line				
Distance (m)	*Left NaI(Tl)*	*Right NaI(Tl)*	*Front NaI(Tl)*	*HPGe*
20	822 ± 4%	834 ± 4%	41.9 ± 4%	94.2 ± 4%
40	174 ± 4%	177 ± 4%	14.6 ± 4%	21.4 ± 4%
80	30.6 ± 4%	31.4 ± 4%	2.85 ± 4%	3.58 ± 4%
120	9.88 ± 4%	9.58 ± 4%	no data	1.10 ± 4%
Co-60 cps/GBq for 1173.2 keV line (NaITl) and for 1332.5 keV line (HPGe)				
Distance (m)	*Left NaI(Tl)*	*Right NaI(Tl)*	*Front NaI(Tl)*	*HPGe*
20	630 ± 5%	640 ± 5%	19.5 ± 6%	56.7 ± 5%
40	138 ± 5%	141 ± 5%	6.59 ± 6%	13.2 ± 5%
80	24.9 ± 5%	27.0 ± 5%	1.58 ± 8%	2.39 ± 6%
160	3.77 ± 7%	3.55 ± 7%	0.196 ± 29%	0.320 ± 9%

Gamma rays are absorbed in air as the detector source distance increases. The count rate per GBq at distance x is related to the count rate I_0 at distance x_0 [6].

$$I(x) = \frac{I_0 x_0^2 e^{-\mu(x-x_0)}}{x^2} \tag{14}$$

where μ is the linear attenuation coefficient in air for a given gamma ray energy. Some relevant values of μ in dry air at sea level are presented in Table V. Data from Table IV is presented in Figures 14–17 together with the theoretical attenuation curves from Equation (14) for each detector type. The curve is normalised to pass the data points at x = 40m. The source was placed perpendicularly to the detector for all measurements. Apart from Am-241, the results from left and right NaI(Tl) sit nicely on the theoretical curve. The front detector is more ambiguous. The deviation with Am-241 could be explained by an alteration in weather conditions: the measurements at 20 and 40 m were done in dense rain and the measurements at 80 and 120 m in clear weather.

A simple approach to evaluating the minimum detectable activity (*MDA*) as a function of distance between the source and the detector is to consider only the statistical fluctuations.

Table V. Values for linear attenuation coefficient μ in dry air as a function of gamma line energy. Calculated from data given in reference [7].

Gamma line energy (keV)	Nuclide	m (1/m)
59.54	Am-241	0.0242
140.5	Tc-99m	0.0175
186.2	Ra-226	0.0163
316.5	Ir-192	0.0135
364.5	I-131	0.0128
468.1	Ir-192	0.0116
661.7	Cs-137	0.0100
1173.2	Co-60	0.0076
1332.5	Co-60	0.0071
1460.8	K-40	0.0068
2614.5	Tl-208	0.0051

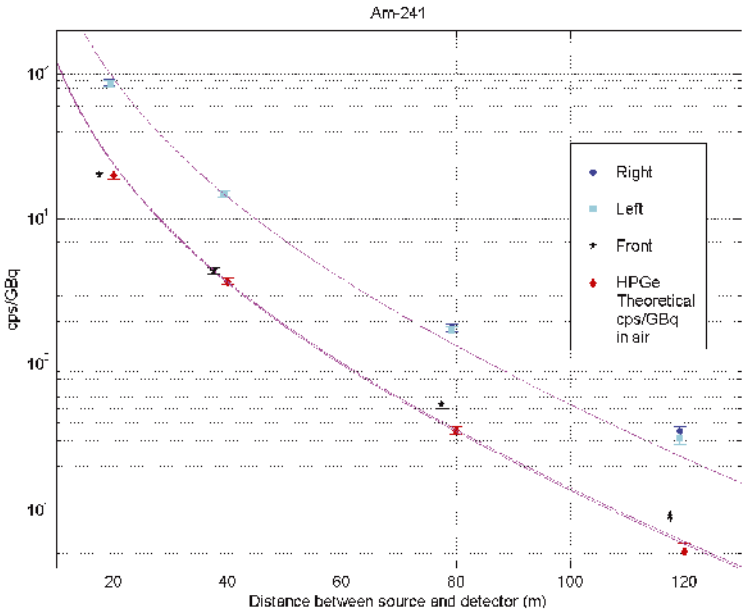

Fig. 14. Count rates of Am-241 at different distances. Alternating weather.

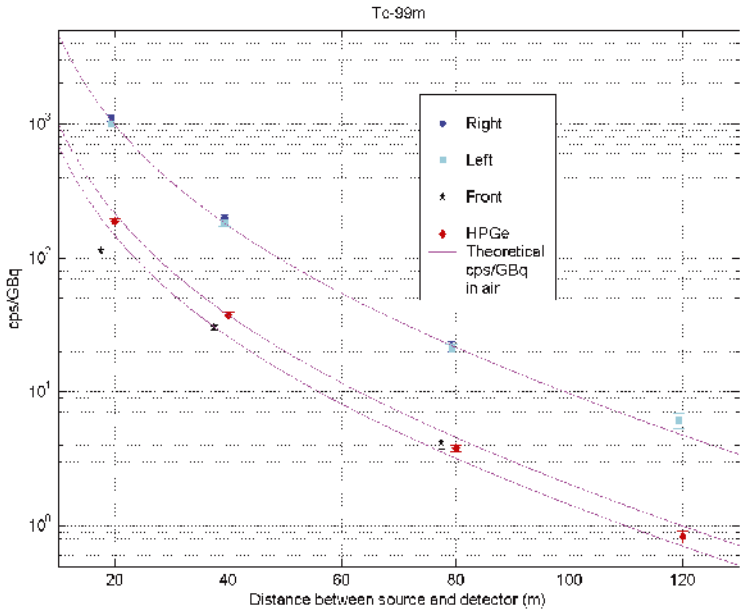

Fig. 15. Decay-corrected count rates of Tc-99m at different distances.

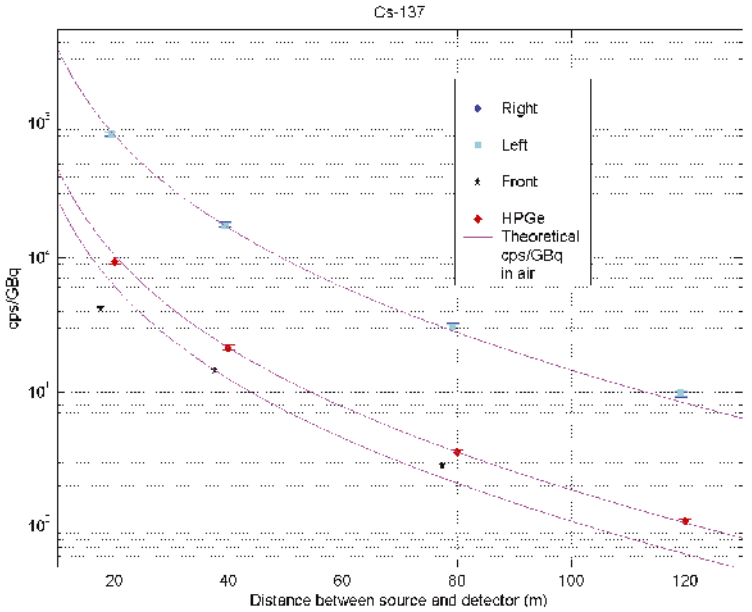

Fig. 16. Count rates of Cs-137 at different distances. Cs-137 from Chernobyl fallout is eliminated.

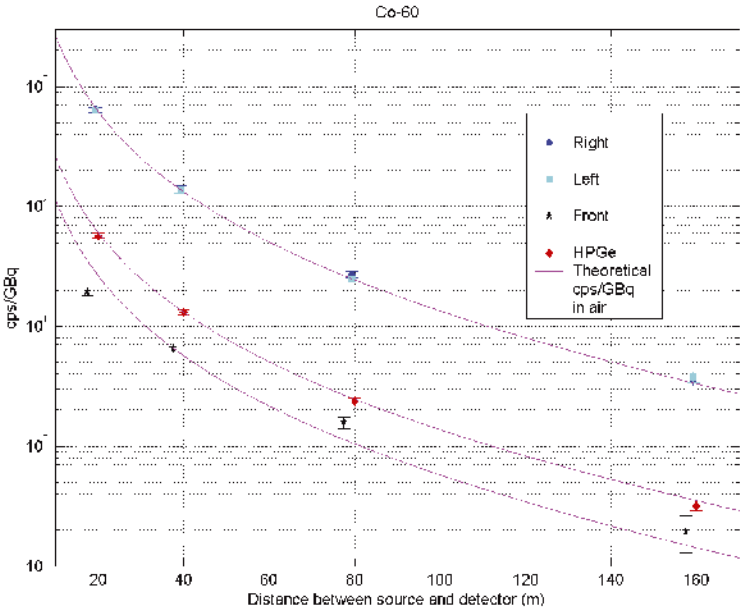

Fig. 17. Count ratess of Co-60 at different distances.

Currie's detection limit is defined as [5]

$$L_D = L_C + \frac{k_\beta^2}{2}\left[1 + \sqrt{1 + \frac{4}{k_\beta^2}\left[L_C + \left(\frac{L_C}{k_\alpha}\right)^2\right]}\right] \tag{15}$$

where k_β defines the risk level for false negatives. The Equation (15) is commonly simplified to

$$L_D = k^2 + 2L_C \tag{16}$$

where an equal risk is taken for both type 1 (false positive) and type 2 (false negative) errors, i.e. $k = k_\alpha = k_\beta$. A very common choice for both risk levels is 5%. However, this is not a suitable setting for false positives in these kinds of security applications due to the large number of false alerts that seriously disturb an operational survey. Hence the low type 1 error risk was chosen, in terms of Gaussian abscissa, $k_\alpha = 4.753$. The type 2 error risk can be essentially higher as it only has impact on Minimum Detectable Activity (*MDA*). Therefore, the common choice of 5 % risk level is made for false negatives, i.e. $k_\beta = 1.645$.

Equation (15) can be simplified through a series expansion:

$$L_D \approx \frac{k_\beta}{2}\left(k_\alpha + k_\beta\right) + \left(1 + \frac{k_\beta}{k_\alpha}\right)L_C \tag{17}$$

Equation (17) is a good approximation for Equation (15). The difference is less than 2% for $L_C > 20$ and it approaches the correct value at larger L_C values.

Currie's theory is based on Gaussian approximation, which is not valid at low counts. For $L_C > 20$ counts, Equation (17) can be further simplified to

$$L_D \approx \left(1 + \frac{k_\beta}{k_\alpha}\right)L_C \tag{18}$$

which gives $L_D = 1.35 * L_C$. This means that peak significance $S = 1.35$ refers to *MDA* in calibration measurements performed with SONNI.

Since the detected peak area A is related to source activity a through

$$A = f\varepsilon Ta \tag{19}$$

where f is the radiation yield per disintegration, ε is the absolute detection efficiency and T the counting time, Equation (8) can be written in the form

$$S - S_{offset} = \frac{f \varepsilon T a}{c L_C(\alpha)} \tag{20}$$

On the other hand, we have stated that for minimum detectable activity *MDA*

$$1.35 = \frac{f \varepsilon T MDA}{c L_C(\alpha)} \tag{21}$$

Hence, for a known activity a_0 and a measured significance S_0 we get

$$\frac{f \varepsilon T}{L_C(\alpha)} = \frac{S_0 - S_{offset}}{a_0} c \tag{22}$$

and by substituting Equation (19) with Equation (22) we get

$$MDA = \frac{1.35 a_0}{S_0 - S_{offset}} \tag{23}$$

Table VI presents the maximum detected significances for right NaI(Tl) and HPGe detectors from sweeps past the radiation sources at Vesivehmaa airfield. Each source was placed at 20, 40 and 80 (Cobalt also at 160) meters from origo located in the middle of an airfield taxiway (see Fig. 18). The spectra were recorded during the drive from one end of the taxiway to the other at speeds of 30 km/h and 60 km/h. All detectors were operated in the 5-second mode.

The significances, activities and significance offsets given in Table VI were used to calculate the *MDA* for the 30 km/h speed with Equation (23). For static measurements, the same original data used to calculate the cps/GBq presented in Table IV was deployed. *MDA* values for right NaI(Tl) are presented in Figures 19–22. The *MDA* estimate for HPGe is given for comparison, but the results for 30 km/h must be treated with great care due to the low count rate issues in 5-second measurements explained in Chapter 3.3.3. Only the uncertainty of the source activity and the measured peak area is taken into account in the total uncertainty estimate. The distribution of counts between consecutive measurements has a significant effect on the *MDA*s for moving survey. If the car hits the origo in the middle of a measurement, a far greater signal is received than if the car hits the origo between two measurements. No effort was made to

Table VI. Maximum significances measured at Vesivehmaa airfield as a function of source to origo distance.

Am-241			
Right NaI (S_{offset} = 0.024)			
Distance (m)	*Source activity (GBq)*	*Detected maximum significance for 59.54 keV line*	
		30 km/h	*60 km/h*
20	42.2	16.847	12.810
40	42.2	8.276	6.447
80	42.2	2.524	2.264
HPGe (S_{offset} = 0.042)			
Distance (m)	*Source activity (GBq)*	*Detected maximum significance for 59.54 keV line*	
		30 km/h	*60 km/h*
20	42.2	4.453	3.584
40	42.2	1.999	1.927
80	42.2	0.679	0.344
Tc-99m			
Right NaI (S_{offset} = 0.255)			
Distance (m)	*Source activity (GBq)*	*Detected maximum significance for 140.5 keV line*	
		30 km/h	*60 km/h*
20	1.34	9.467	6.617
40	1.28	3.939	3.259
80	1.17	1.063	0.752
HPGe (S_{offset} = 0.044)			
Distance (m)	*Source activity (GBq)*	*Detected maximum significance for 140.5 keV line*	
		30 km/h	*60 km/h*
20	1.34	5.085	3.161
40	1.28	2.386	1.818
80	1.17	0.684	0.480

Cs-137			
Right NaI (S_{offset} = 1.114)			
Distance (m)	*Source activity (GBq)*	*Detected maximum significance for 661.7 keV line*	
		30 km/h	*60 km/h*
20	3.18	15.110	12.216
40	3.18	7.433	7.086
80	3.18	3.754	3.152
HPGe (S_{offset} = 0.616)			
Distance (m)	*Source activity (GBq)*	*Detected maximum significance for 661.7 keV line*	
		30 km/h	*60 km/h*
20	3.18	5.653	5.034
40	3.18	3.381	2.867
80	3.18	1.677	1.466
Co-60			
Right NaI (S_{offset} = 0.160)			
Distance (m)	*Source activity (GBq)*	*Detected maximum significance for 1173 keV line*	
		30 km/h	*60 km/h*
20	1.78	8.261	6.076
40	1.78	4.272	3.134
80	1.78	2.025	1.618
160	1.78	0.661	0.640
HPGe (S_{offset} = 0.006)			
Distance (m)	*Source activity (GBq)*	*Detected maximum significance for 1173 keV line*	
		30 km/h	*60 km/h*
20	1.78	3.514	3.273
40	1.78	2.333	1.907
80	1.78	1.090	0.893
160	1.78	0.726	0.467

synchronise the measurements with the passing of the origo since no such thing is possible in a real situation.

Detection distances for open Co-60 source that exceed the activity level of high-activity sealed radioactive sources (HASS) listed in the Council Directive 2003/122/EURATOM [8] are given in Table VII.

Table VII. Detection distances for HASS activity level of Co-60.

Driving speed 30 km/h , 5 seconds acquisition time					
Nuclide	*HASS activity (GBq)*	*Detection distance, source to origo (m)*			
		Right NaI		*HPGe*	
Co-60	4	120		90	
Immobile measurement, 500 seconds acquisition time					
Nuclide	*HASS activity (GBq)*	*Detection distance, source to origo (m) *)*			
		Left NaI	*Right NaI*	*HPGe*	*Front NaI*
Co-60	4	260	260	250	155

*) Crude extrapolation.

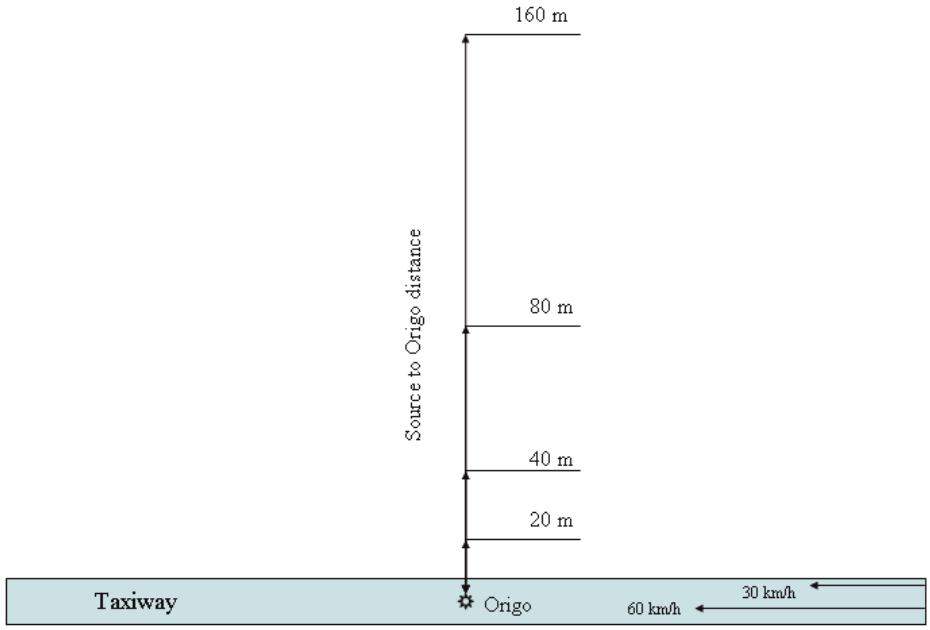

Fig. 18. Test setup for determining the detection distances in a 5-second operating mode at the airfield.

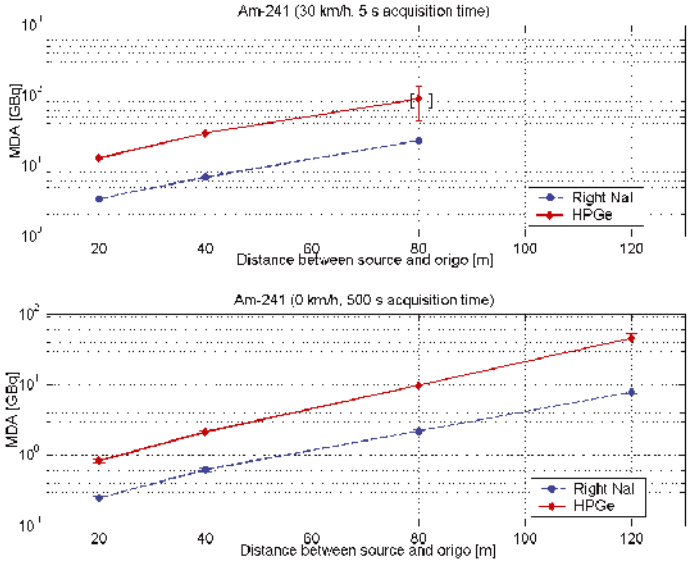

Fig. 19. *MDA* for Am-241 with 30 km/h driving speed and 5-second acquisition time as a function of distance between source and origo compared to results with car parked and 500-second acquisition time. Measurements with $S < 1$ are marked with square brackets ([ ]).

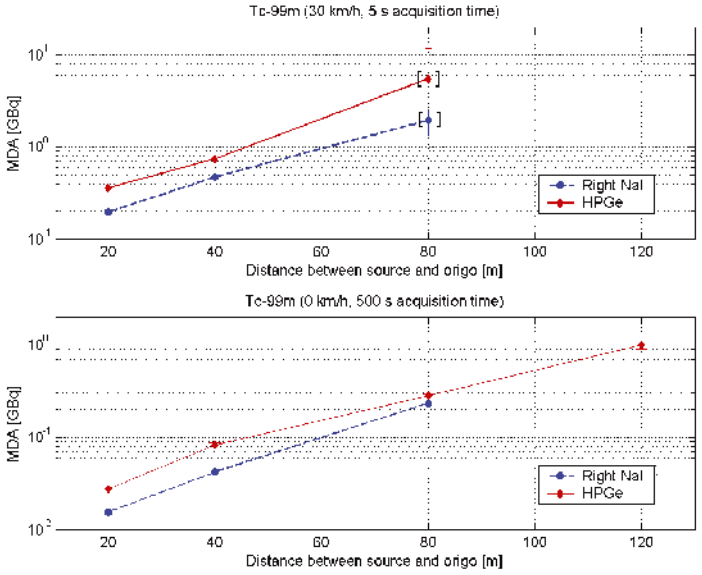

Fig. 20. *MDA* for Tc-99m with 30 km/h driving speed and 5-second acquisition time as a function of distance between source and origo compared to results with car parked and 500-second acquisition time. Measurements with $S < 1$ are marked with square brackets ([ ]).

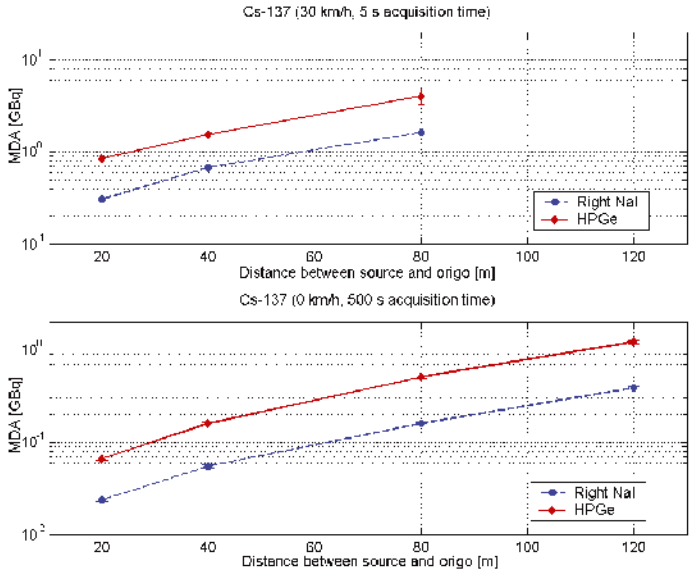

Fig. 21. *MDA* for Cs-137 with 30 km/h driving speed and 5-second acquisition time as a function of distance between source and origo compared to results with car parked and 500-second acquisition time.

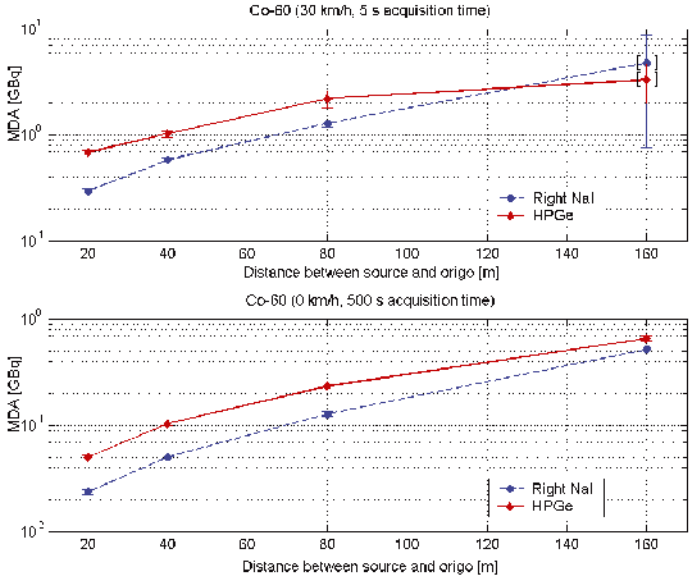

Fig. 22. *MDA* for Co-60 with 30 km/h driving speed and 5-second acquisition time as a function of distance between source and origo compared to results with car parked and 500-second acquisition time. Measurements with $S < 1$ are marked with square brackets ([ ]).

4.2 Ir-192

Measurements for determining the net peak count rate per GBq for Iridium-192 were repeated with the left NaI(Tl) and HPGe detectors at Vesivehmaa airfield. The error estimates are dominated by the uncertainty of the source activity, which was approximately 20% due to a non-existent calibration certificate, therefore lacking details of the geometrics of the source. The Ir-192 source was partially shielded during the measurements. Hence the results presented in Table VIII should not be applied together with the results given in Table IV for efficiency calculations.

Table VIII. Net count rate per GBq as a function of distance between source and origo for Ir-192 316.5 and 468.1 keV lines. For NaI(Tl) detectors, the 316.5keV peak incorporates the 308.5 and 295.96 keV Ir-192 peaks as well. Similarly, the 484.6 keV peak is included in the 468.1keV peak.

Ir-192 cps/GBq for 316.5 keV line		
Distance (m)	*Left NaI(Tl)*	*HPGe*
20	549.839 ± 22%	73.3 ± 22%
40	151.698 ± 22%	14.5 ± 22%
60	42.33409 ± 22%	4.34 ± 22%
70	22.83164 ± 22%	2.21 ± 22%
80	17.30558 ± 22%	1.63 ± 23%
100	6.283168 ± 22%	0.572 ± 22%
120	1.952477 ± 23%	0.193 ± 23%
140	2.000407 ± 23%	0.111 ± 23%
180	0.436766 ± 32%	0.0420 ± 25%
Ir-192 cps/GBq for 468.1 keV line		
Distance (m)	*Left NaI(Tl)*	*HPGe*
20	346 ± 22%	49.0 ± 22%
40	89.0 ± 22%	9.72 ± 22%
60	27.8 ± 22%	3.03 ± 22%
70	16.0 ± 22%	1.72 ± 22%
80	11.5 ± 23%	1.30 ± 22%
100	5.02 ± 22%	0.492 ± 22%
120	1.98 ± 22%	0.194 ± 23%
140	1.12 ± 23%	0.105 ± 23%
180	0.558 ± 25%	0.0522 ± 24%

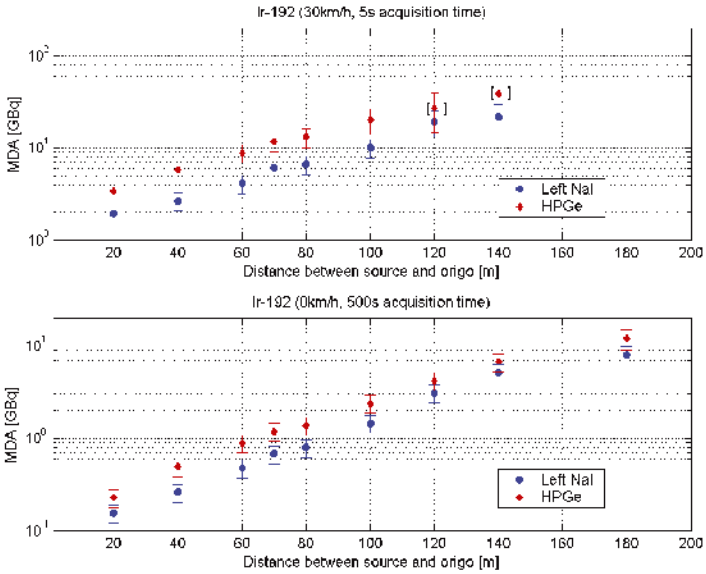

Fig. 23. *MDA* for Ir-192 with 30 km/h driving speed and 5-second acquisition time as a function of distance between source and origo compared to results with car parked and 500-second acquisition time. Measurements with $S < 1$ are marked with square brackets ([ ]). The 468.1 keV line was used for the calculations.

5 Automated SDS messages

An SDS (Short Data Service) message is a text message that can be sent via the TETRA-based Public Authorities Network called VIRVE in Finland. An SDS message may contain up to 140 characters. The transmission of SDS messages from SONNI to headquarters is fully automated. The hypothesis test result (peak significance above a certain threshold) is the triggering signal for SDS transmission.

When the alarm limit defined in the initialisation file is exceeded, the analysis script produces an alarm. These alarms are sent to the *communications* database in Lille (described in Appendix 1). Each alarm is saved as one entry in the *alarms* table containing information about the alarm type (e.g. the detected nuclide), alarmed detector, significance, net count rate, position information and signal level. If nothing is detected, a specific *NULL*-alarm is updated in the *alarms* table. This entry specifies the latest measurement with normal background.

The criteria for sending the messages to a certain recipient are stored in the *communications* database, which also contains information on the name, address and transmission method. Each recipient of automated messages is associated with limits for signal level, the number of times the signal level has to be exceeded and the minimum configuration of alarmed detectors. A specific perlscript called *messaging* compares the data in the *alarms* table with the limits in the *recipients* table.

The messaging script is executed once every two seconds. First it checks the *flags* table to see if the detectors are being calibrated or if the system is being tested. No messages are sent during calibration, whereas the word “TEST” is added to the SDS messages during testing. The *test* and *calibration* flags can be set from the command line when necessary. If there are no calibrations ongoing, the script fetches the maximum significance level for all the alarms generated after the latest *NULL*-alarm. The next stage is to fetch the limits for sending messages for each active recipient and start comparing the limits to the alarms. The first criterion to compare is the number of generated alarms that have a significance level bigger than the limit stored in the *recipients* table. If the limit is exceeded, the script compares the configuration of alarmed detectors to the needed minimum configuration. There are three different options: any of the detectors, HPGe and one of the NaI(Tl) detectors, or all detectors. Demanding simultaneous identification from HPGe and one of the NaI(Tl) detectors is an efficient method for excluding false positives caused by microphonics in HPGe or wrong identifications in NaI(Tl) because of the poor resolution. The last thing before writing a message is to check whether there already is a message on the

same observation written in the *messages* table for the same *recipient*. If true, the message is not sent unless the time gap between the existing and the new message exceeds the time limit specified in the *recipients* table.

An example of an SDS message is presented below.

11:47:54 UTC
15Jun2005
SONNI
Cs-137 ident
24.81609
60.20985
auto
L:S2.3 c66
I:S1.0 c5
id = 14
WGS84

This message indicates that at *11:47:54 UTC* on the *15th of June, 2005* *SONNI* has found and *ident*ified*) *Cs-137* at latitude *60.20985* and longitude *24.81609* and *auto*matically generated this message. The nuclide was detected with both the left NaI(Tl) and the *in-situ* HPGe detector. The calculated significances and net count rates are *2.3* and *66* for NaI(Tl) and *1.0* and *5* for HPGe. The message identification number is *14* in the *communications* database. Coordinates are given in *WGS84*.

While the messaging script scans the alarms table, another script for sending the SDS messages scans the messages table. Every time a new SDS message is detected in the database, the SDS sending script sends it to its receiver via VIRVE and marks the message as sent in the database.

*) A nuclide is only marked *ident*ified if it is detected with both HPGe and at least one of the NaI(Tl) detectors and the criterion $S > 1$ is met. A weak signal detected with only one of the detectors is marked as a *poss*ible finding. Any observation with a high significance level should be detected with more than just one detector. Hence a finding with only one of the detectors is marked *prob*able, even if the significance level $S > 1$ is breached.

6 Discussion

The summation algorithm presented in this paper has been in use during several security surveillance missions in Finland. It has proven to be fast and reliable in real-time analyses [9][10]. However, some optimisation is still needed. The algorithm cannot be used as such with low efficiency detectors or in circumstances with a very low background where Gaussian statistics do not apply. This will be corrected in the near future by applying Poissonian statistics to these cases. Another weak point is that the low risk setting for type 1 alarms makes it insensitive to very small signals. In 2006, a comparison of in-house processing methods used in urban gamma spectrometry, was carried out between the Technical University of Denmark (DTU) and STUK [11]. The results showed that, in comparison with methods based on area-specific spectrum stripping (ASSS) or fitting with spectral components (FSC) used and developed by the DTU, the peak significance calculation proved to be more insensitive, although with better control of statistics and with easier mathematics applied. Clearly, the algorithm can be made more powerful by including the measurement history in the analysis, as is done in the FSC-based methods.

7 References

1. Smolander P, Toivonen H. Mobile in-field measurements in nuclear or radiological threat situations. IRPA11 conference, Madrid (2004): http://irpa11.irpa.net/pdfs/7a24.pdf
2. Doletum Oy Ltd. UniSAMPO – Advanced gamma spectrum analysis software, version 2.2. User's guide. Helsinki: 2004.
3. Comprehensive nuclear test-ban-treaty organization, formats and protocols for messages. IDC-3.4.1 Rev3. Vienna: 2001.
4. Aarnio P. LINSSI – SQL Database for gamma-ray spectrometry – Part I: DATABASE, Version 1.1. Helsinki University of Technology; Espoo: 2005.
5. Currie L. Limits for qualitative detection and quantitative determination. Analytical Chemistry 1968; 40.
6. Knoll G. Radiation detection and measurements. 3rd edition. John Wiley & Sons; 2000. p. 53–54.
7. Hubbell J, Seltzer S. Tables of X-ray mass attenuation coefficients and mass energy-absorption coefficients. National Institute of Standards and Technology (NIST) 1996. <http://physics.nist.gov/PhysRefData/XrayMassCoef/cover.html>
8. Council directive 2003/122/Euratom, Annex I. 2003.
9. Toivonen H, Kuukankorpi S, Moring M, Smolander P. Radionuclide source finding using a mobile laboratory for supporting counter terrorism actions, in: Maatela P, Pitkänen M (eds.). NBC 2006 Symposium on chemical, biological, nuclear and radiological threats – a safety and security challenge. Tampere, Finland; 2006.
10. Smolander P, Kuukankorpi S, Moring M, Toivonen H. In-field data management in radiological threat and emergency. In: Proceedings of MARC VII. 2006. To be published in the Journal of Radioanalytical and Nuclear Chemistry in 2008.
11. Aage H, Kuukankorpi S, Moring M, Smolander P, Toivonen H. Urban gamma spectrometry – Final report. NKS Nordic Nuclear Safety Report. Report from the AFT/B(06)3 project group. 2006.

APPENDIX 1
DATABASE FOR COMMUNICATION PURPOSES IN SONNI

This appendix describes the *communications* database designed for automated data communication from SONNI.

The *communications* database comprises seven tables: *recipients*, *messages*, *errors*, *messageReference*, *alarms*, *flags* and *flagLog*, which are all described on the following pages:

A.1 Alarms

The analysis script writes key information on observations that exceed the decision limit in the *alarms* table.

Table A.1. The *alarms* table structure

alarms			
Field	*Type*	*Key*	*Default/Options*
idAlarm	int(11)	P AI	NULL
alarmType	varchar(7)		NULL/nuclideId/ total/hiEnd
source	char(1)		I/L/R/F
idMeas	int(11)	F	0
idAnalysis	int(11)	F	0
significance	double(8,1)		NULL
SLevel	enum(L/M)		NULL
cps	double(8)		NULL
acqEnd	datetime		NULL
latitude	double(8,5)		NULL
longitude	double(8,5)		NULL

idAlarm Identification number for the alarm. Used to link the generated messages to original alarms and measurements with the *messageReference* table. Alarms with *idAlarm* numbers 1 to 4 are so called NULL-alarms, one for each *in situ* detector. These are updated when nothing is detected.

alarmType Type of alarm. Options are: detected nuclide (nuclideId), total pulse rate (total), pulse rate at high energies (hiEnd) or NULL for the NULL-alarms.

source Alarmed detector. Options are I for *in situ* HPGe and L for left, R for right and F for front NaI(Tl) detectors.

idMeas Identification number for the analysed measurement in *measurements* table in Linssi v1.1 database

idAnalysis Identification number for the analysis that generated this alarm in *analyses* table in Linssi v1.1 database

significance Significance for detected nuclide.

SLevel Relative intensity for the signal as defined in the initialization file for the analysis. So far the options are Low for internal alerts and Medium for external signals.

cps Net count rate for the nuclide peak or total count rate or high energy count rate depending on the *alarmType*.

acqEnd The acquisition end time for the measurement identified by *idMeas*.

latitude Latitude for the vehicle at *acqEnd*.

longitude Longitude for the vehicle at *acqEnd*.

A.2 Flags

The *flags* table is used to communicate ongoing calibrations or tests to the messaging script. The flags are set from the command line.

Table A.2. The *flags* table structure

flags			
Field	*Type*	*Key*	*Default*
calibration	tinyint(1)		0
test	tinyint(1)		0

calibration Set TRUE for ongoing calibrations. If TRUE, no messages are sent.

test Set TRUE for running tests. If TRUE, messages are sent only to those recipients with *parReportTests* = TRUE.

A.3 FlagLog

The *flagLog* table is used to track changes in the state of the flags.

Table A.3. The *flagLog* table structure.

flagLog			
Field	*Type*	*Key*	*Default*
flagName	varchar(20)		NULL
setTime	datetime		NULL
setTo	tinyint(1)		NULL

flagName Name of the field in the *flags* table that got changed
setTime Time the change was made
setTo New state for the flag

A.4 Recipients

The *recipients* table covers name and address information on the recipients for automated messages. All fields starting with *par* are parameters for controlling the messaging script.

Table A.4. The *recipients* table structure.

recipients			
Field	*Type*	*Key*	*Default/Options*
idRecipient	int(5)	P AI	NULL
recipientName	varchar(40)	U	NULL
method	varchar(10)		NOT NULL
address	varchar(80)		NULL
parReportTests	tinyint(1)		0
parMessageSent	int(5)		60
parSLevel	enum(L/M)		M
parTimesOverSLevel	int(5)		1
parIdentDetectors	enum(single/ both/all)		both
parAddInfo	enum(S/cps/both)		NULL
inUse	tinyint(1)		1

idRecipient Identification number for the recipient.

recipientName Name of the recipient.

method Way of communication. For example, SDS for text messages, sound for notifying the SONNI crew.

address Recipient's address. If *method* is SDS, this is a VIRVE phone number.

parReportTests If FALSE, this recipient won't get any messages during tests. If TRUE, messages are sent also during tests but the messages begin with line *SONNI TEST*.

parMessageSent Seconds to wait before repeating a message if the same alarms are repeated.

parSLevel Minimum signal level to be reported. Options are the same in the *alarms* table.

parTimesOverSLevel Minimum number of consecutive signals with signal level >= *parSLevel* required for report to be sent.

parIdentDetectors Minimum configuration of alarmed detectors required for reporting. Options are: *single* for any of the four detectors, *both* for HPGe and one of the NaI(Tl) detectors and *all* for all four detectors. Note that if a configuration of several detectors is required, only one detector has to exceed the minimum signal level *parSLevel parTimesOverSLevel* times for reporting.

parAddInfo This parameter is used to define what additional info will be written in the end of the message. Options are: *s* for significance info, *cps* for pulse rate info and *both* for both. If the total pulse rate is reported, the significance will be marked as 0.0. The chosen information is listed from all alarmed detectors.

inUse Flag used to temporarily exclude (*inUse* = FALSE) the recipient from the group of message receivers without deleting the recipient information from the database.

A.5 Messages

The *messages* table is used to store all the messages that are generated in SONNI.

Table A.5. The *messages* table structure.

messages			
Field	*Type*	*Key*	*Default*
idMessage	int(11)	P AI	NULL
idRecipient	int(5)	F	NOT NULL
recipientName	varchar(40)		NULL
method	varchar(10)		NULL
address	varchar(80)		NULL
sender	varchar(40)	MUL1	NULL
senderReference	varchar(20)	MUL1	NULL
creationTime	datetime	MUL2	0000-00-00 00:00:00
transmitTime	datetime		NULL
errors	tinyint(1)		0
message	longblob		NULL
comments	varchar(80)		NULL

idMessage Identification number for the message.

idRecipient Identification of number of the recipient. Key to the *recipients* table. If the message is generated manually to a recipient not included in the *recipients* table, the *recipientName*, *method* and *address* field are inserted straight to the *messages* table. Otherwise this information is fetched from the *recipients* table.

recipientName See *recipients* table.

method See *recipients* table.

address See *recipients* table.

sender Creator of this message. May be either a person or a program.

senderReference Reference to the message origin. With automatically created messages the *senderReference* put together with identification number of the recipient of the message, alarm type and the confidence level of the signal.

creationTime Message creation date and time.

transmitTime Message transmit date and time. If set to NULL, the message has not been sent.

errors If TRUE there are errors associated to the message or to its transmission.

message The message body.

comments A field for comments.

A.6 MessageReference

This table is used to link the messages with the alarms that caused the message to be written.

Table A.6. The *messageReference* table structure.

messageReference			
Field	*Type*	*Key*	*Default*
idMessage	int(11)	F	0
idAlarm	int(11)	F	0

idMessage Identification number of the message. Key to the *messages* table.

idAlarm Identification number for the alarm used to generate the message. Key to the *alarms* table.

A.7 Errors

This table is used for storing any errors that might occur when sending the messages.

Table A.7. The *errors* table structure.

errors			
Field	*Type*	*Key*	*Default*
idError	int(11)	P AI	NULL
idMessage	int(11)	F	NULL
errorTime	datetime		NULL
errorText	text		NULL

idError Identification number for the error.
idMessage Identification number for the erraneous message, Key to the messages table.
errorTime Time of the error.
errorText Description of the error.

STUK-A-reports

STUK-A224 Kuukankorpi S, Toivonen H, Moring M, Smolander P. Mobile spectrometry system for source finding and prompt reporting. Helsinki 2007.

STUK-A223 Jussila P. Thermomechanics of swelling unsaturated porous media. Compacted bentonite clay in spent fuel disposal. ScD Thesis. Helsinki 2007.

STUK-A222 Hutri K-L. An approach to palaeoseismicity in the Olkiluoto (sea) area during the early Holocene. PhD thesis. Helsinki 2007.

STUK-A221 Valmari T, Arvela H, Reisbacka H. Päiväkotien radonkartoitus. Helsinki 2007.

STUK-A220 Karppinen J, Järvinen H. Tietokonetomografialaitteiden käytön optimointi. Helsinki 2006.

STUK-A219 Tapiovaara M. Relationships between Physical Measurements and User Evaluation of Image Quality in Medical Radiology – a Review. Helsinki 2006.

STUK-A218 Ikäheimonen TK, Klemola S, Ilus E, Vartti V-P, Mattila J. Monitoring of radionuclides in the vicinities of Finnish nuclear power plants in 1999–2001. Helsinki 2006.

STUK-A217 Ikäheimonen TK (toim.). Ympäristön radioaktiivisuus Suomessa – 20 vuotta Tshernobylista. Symposium Helsingissä 25.–26.4.2006. Helsinki 2006.

STUK-A216 Pastila R. Effect of long-wave UV radiation on mouse melanoma: An in vitro and in vivo study. Doctoral thesis. Helsinki 2006.

STUK-A215 Rantavaara A. Elintarvikeketjun suojaustoimenpiteet laskeumatilanteiden varalle. Helsinki 2005.

STUK-A214 Sinkko K, Ammann M, Hämäläinen RP, Mustajoki J. Facilitated workshop on clean-up actions in inhabited areas in Finland after an accidental release of radionuclides. Helsinki 2005.

STUK-A213 Vesterbacka P. ^{238}U–series radionuclides in Finnish groundwater-based drinking water and effective doses. Helsinki 2005.

STUK-A212 Kantala T. Elintarvike-teollisuuslaitosten ja niiden ympäristön puhdistustoimenpiteet säteilytilanteessa. Helsinki 2005.

STUK-A211 Muikku M, Arvela H, Järvinen H, Korpela H, Kostiainen E, Mäkeläinen I, Vartiainen E, Vesterbacka K. Annoskakku 2004 – suomalaisten keskimääräinen efektiivinen annos. Helsinki 2005.

STUK-A210 Salomaa S, Ikäheimonen TK (eds.). Research activities of STUK 2000–2004. Helsinki 2005.

STUK-A209 Valmari T, Rantavaara A, Hänninen R. Radioaktiivisten aineiden siirtyminen päästöpilven kulkeutumisen aikana tuotettaviin elintarvikkeisiin. Helsinki 2004.

STUK-A208 Kiuru A. Molecular biology methods in assessing radiation-induced hereditary risks in humans. Helsinki 2004

STUK-A207 Sinkko K. Nuclear emergency response planning based on participatory decision analytic approaches. Helsinki 2004.

STUK-A206 Hämäläinen K, Vesterbacka P, Mäkeläinen I, Arvela H. Vesilaitosten vedenkäsittelyn vaikutus luonnon radionuklidipitoisuuksiin (VEERA). Helsinki 2004.

STUK-A205 Klemola S, Ilus E, Ikäheimonen TK. Monitoring of radionuclides in the vicinities of Finnish nuclear power plants in 1997 and 1998. Helsinki 2004.

STUK-A204 Kettunen A. Radiation dose and radiation risk to foetuses and newborns during x-ray examinations. Helsinki 2004.

STUK-A203 Rahola T, Etherington G, Bérard P, Le Guen B, Hurtgen C, Muikku M, Pusa S. Survey of Internal Dose Monitoring Programmes for Radiation Workers. WP 1 in the project OMINEX (Optimisation of Monitoring for Internal Exposure). Helsinki 2003.

STUK-A202 Salomaa S (ed.). Research projects of STUK 2003–2005. Helsinki 2004.

STUK-A201 Mäkeläinen I (toim.). Säteilyn ja kemiallisten aineiden riski-filosofiat ja suojeluperusteet. Helsinki 2003.

STUK-A200 Vetikko V, Valmari T, Oksanen M, Rantavaara A, Klemola S, Hänninen R. Energiateollisuudessa syntyvän puuntuhkan radioaktiivisuus ja sen säteilyvaikutukset. Helsinki 2004.

STUK-A reports
on STUK's home pages:
www.stuk.fi/julkaisut_maaraykset/en_GB/listaus/?year=&type=&series=STUK-A

A

STUK
Laippatie 4, 00880 Helsinki
Puh. (09) 759 881, fax (09) 759 88 500
www.stuk.fi

ISBN 978-952-478-281-4
ISSN 0781-1705
Edita Prima Oy, Helsinki 2007